CHAPTER 5

Ferrofluid Lubrication of Porous Journal Bearing with Variable Magnetic Field

CONTENTS

SYMBOLS

c	radial clearance (m)
e	eccentricity
FF	ferrofluid
h	film thickness (m)
$\dot{h}$	squeeze velocity, dh/dt $(\mathrm{m\,s^{-1}})$
H	magnetic field vector
H	magnetic field strength (magnitude of **H**) (A $\mathrm{m^{-1}}$)
H^*	thickness of the porous facing (m)
$\bar{H}^*$	dimensionless porous thickness parameter defined as $(\bar{H}^* = H^*/c)$
I	sum of moments of inertia of the particles per unit volume (N $\mathrm{s^2\,m^{-2}}$)
k	quantity chosen to suit the dimensions of both sides of equation (5.24) ($\mathrm{A^2\,m^{-4}}$)
k_B	Boltzmann's constant $(\mathrm{J\,(^oK)^{-1}})$
L	length of the bearing (m)
m	magnetic moment of a particle (A $\mathrm{m^2}$)
M	magnetization vector
$\mathbf{M}_0$	equilibrium magnetization (A $\mathrm{m^{-1}}$); $\xi = mH/k_BT$
M	magnitude of **M**
MF	magnetic fluid
n	number of magnetic particles per unit volume ($\mathrm{m^{-3}}$)
p	fluid pressure in the film region (N $\mathrm{m^{-2}}$)
P	fluid pressure in the porous region (N $\mathrm{m^{-2}}$)
R	radius of the journal (m)

s	slip constant (m^{-1})
$\mathbf{S}$	sum of angular momentums of particles per unit volume ($K\ m^2\ s^{-1}$)
t	time (s)
T	temperature (^oK)
u , w	velocity components in the film region in the x and z – directions, respectively ($m\ s^{-1}$)
$\bar{u}, \bar{w}$	velocity components in the porous region in the x and z – directions, respectively ($m\ s^{-1}$)
$\mathbf{q}$	fluid velocity vector
V	volume of the particle (m^3)
VMF	variable magnetic field
W	load-carrying capacity (N)
$\overline{W}$	dimensionless load-carrying capacity defined in equation (5.29)
x, y, z	co-ordinates (m)

Greek symbols

α	inclination of the magnetic field with the x – axis
ε	eccentricity ratio
μ_0	permeability of free space ($N\ A^{-2}$)
η	viscosity of the suspension ($N\ s\ m^{-2}$)
η_0	viscosity of the carrier liquid ($N\ s\ m^{-2}$)
η_x	porosity in the x – direction
ϕ_x	permeability of porous facing in the x – direction ($N\ A^{-2}$)
ϕ_z	permeability of porous facing in the z – direction ($N\ A^{-2}$)
φ	volume concentration of particles

τ_B	Brownian rotational diffusion time (Brownian relaxation time) (s)
τ_s	internal angular momentum relaxation time (s)
ψ	dimensionless permeability parameter
ψ_x	dimensionless permeability parameter in the x – direction defined in equation (5.21)
ψ_z	dimensionless permeability parameter in the z – direction defined in equation (5.21)
ξ	Langvin parameter
$\boldsymbol{\Omega} = \frac{1}{2}\nabla \times \mathbf{q}$	local angular velocity of rotation of the fluid (rad s^{-1})

5.1 INTRODUCTION

Journal bearing consists of a shaft which rotates inside a sleeve with a layer of lubricant separating these two parts. It is designed to support radial load. It is known as journal bearing because neck of the shaft is called journal. When the journal bearings operated under hydrodynamic lubrication conditions, they are known as hydrodynamic journal bearings. They are widely used bearings in the industry because of long life, shock resistance, vibration absorption. It is mostly used in turbo machinery. Following are some recent references of different journal bearings from different viewpoints.

Kuzhir [1] predicted the shape of a Ferrofluid (FF) free boundary in the presence of a static load and magnetic field in journal bearing. It is shown that the lubricant leakage diminished due to magnetic field effect. Patel *et. al.* [2] studied performance of a hydrodynamic short journal bearing. The results show the nominal increase in load-carrying capacity with respect to magnetic parameter while significant increase with respect to eccentricity ratio. Lin *et. al.* [3] investigated short journal bearings using non-Newtonian FFs as lubricant and the micro-continuum theory of Stokes. The results show that bearings can support higher load capacity as compared to conventional lubricant. Comparing with Newtonian FF case, the effects of couple stresses of non-Newtonian FFs enhance load capacity while reduction in the friction parameter. Hsu *et. al.* [4] investigated long journal bearings with the effects of stochastic surface roughness and magnetic field. They also showed transverse roughness enhance film pressure, load capacity, while reduced the attitude angle and modified friction coefficient. The longitudinal roughness shows the opposite effect. Rao *et. al.* [5] analyzed long journal bearing with porous layer using displaced infinitely long wire magnetic field model. Dimensionless load-carrying capacity and coefficient of friction are studied for different parameters like permeability, thickness of porous layer and lubricant layer, magnetic field intensity and distance ratio parameter. The results show the increase in

load-carrying capacity and reduction in coefficient of friction. Hu and Xu [6] mathematically studied lubrication performance of the journal bearing using cohesion forces & couple stresses of MFs, and the effect of squeeze dynamics. The bearing characteristics like load-carrying capacity, attitude angle, friction coefficient and side leakage are studied. The results show that dimensionless load-carrying capacity increases with the increase of squeeze parameter, cohesion force coefficient and couple stress parameter of the Magnetic Fluid (MF). Laghrabli *et. al.* [7] studied finite journal bearings, where a magnetic field is created by displaced finite wire. The results show the increase in pressure, load capacity, attitude angle and side leakage while decrease in friction factor when the value of each control parameter (magnetic force coefficient and viscosity) increased at low and medium eccentricity ratios. However, at high eccentricity ratios the FF viscosity parameter decreases the load capacity and increases the friction factor.

This Chapter discusses the problem of porous journal bearing using variable magnetic field using Shliomis model [8]. The variable and strong magnetic field is used because of retaining contributions from all magnetic terms of the Shliomis model. The modified Reynolds-Darcy equation for porous journal bearing is derived by considering equation of continuity in the film as well as porous region, and by assuming the validity of the Darcy's law in the porous region. While deriving the equation, the effects of squeeze velocity, anisotropic permeability and slip velocity are also included. The expression for dimensionless load-carrying capacity ($\overline{W}$) is obtained from the pressure equation and studied for different parameters.

5.2 Mathematical Formulation of the Problem

Assuming steady flow, neglecting inertia and the second derivative of the internal angular momentum **S**, equations governed by Shliomis becomes [9,10]

$$-\nabla p+\eta\nabla^2\mathbf{q}+\mu_0(\mathbf{M}\cdot\nabla)\mathbf{H}+\frac{1}{2}\mu_0\nabla\times(\mathbf{M}\times\mathbf{H})=\mathbf{0}, \tag{5.1}$$

$$\mathbf{M}=M_0\frac{\mathbf{H}}{H}+\tau_{\mathrm{B}}(\boldsymbol{\Omega}\times\mathbf{M})-\frac{\mu_0\tau_{\mathrm{s}}\tau_{\mathrm{B}}}{I}[\mathbf{M}\times(\mathbf{M}\times\mathbf{H})], \tag{5.2}$$

where

$$M_0=nm\left(\coth\xi-\frac{1}{\xi}\right),\ \xi=\frac{\mu_0 mH}{k_{\mathrm{B}}T}. \tag{5.3}$$

Referring to [8,11], for colloidal suspensions the condition $\Omega\tau_{\mathrm{B}}<<1$ is always satisfied, equation (5.2) then can be approximated as

$$\mathbf{M}=\frac{M_0}{H}[\mathbf{H}+\bar{\tau}(\boldsymbol{\Omega}\times\mathbf{H})], \tag{5.4}$$

where

$$\bar{\tau}=\frac{\tau_{\mathrm{B}}}{1+\frac{\mu_0\tau_{\mathrm{B}}\tau_{\mathrm{s}}}{I}M_0H}. \tag{5.5}$$

Choose an external oblique radially VMF [12]

$$\mathbf{H}=H(x)(\cos\alpha,0,\sin\alpha), \tag{5.6}$$

where α being inclination of the magnetic field with the x – axis. This is the case of a sample magnetic field. Other suitable form of magnetic fields can be chosen similarly as per requirement.

By assuming that the velocity gradient across the film predominate, equation (5.4) for small α, and equation $\boldsymbol{\Omega}=\frac{1}{2}\nabla\times\mathbf{q}$ implies

$$\mathbf{M}\times\mathbf{H}=-M_0H\,\bar{\tau}\,\boldsymbol{\Omega}. \tag{5.7}$$

Under usual assumption of lubrication, the x – component of the equation (5.1), using equation (5.4) and (5.7) becomes

$$\frac{\partial^2 u}{\partial z^2} = \frac{1}{\eta\left(1+\frac{\mu_0 M_0 H\bar{\tau}}{4\eta}\right)}\left(\frac{dp}{dx} - \mu_0 M_0 \frac{dH}{dx}\right), \tag{5.8}$$

where u is velocity component in the film region in the x – direction.

Using (5.3) and defining the following quantities for a suspension of spherical particles [8, 9]

$$\tau_B = \frac{3\eta V}{k_B T}, \varphi = nV, \tau_s = \frac{I}{6\eta\varphi}, \tag{5.9}$$

equation (5.8) takes the form

$$\frac{\partial^2 u}{\partial z^2} = \frac{1}{\eta(1+\tau)}\frac{d}{dx}\left(p - nk_B T \ln\frac{\sinh\xi}{\xi}\right) \tag{5.10}$$

using equation

$$\tau = \frac{3}{2}\varphi\frac{\xi - \tanh\xi}{\xi + \tanh\xi}.$$

5.2.1 MATHEMATICAL MODELING OF FF BASED POROUS JOURNAL BEARING

Figure 5.1 shows physical configuration of the porous journal bearing, where the bearing surface is attached with a porous facing (or porous matrix or porous region or porous layer) of uniform thickness H^* and the journal is a solid surface of radius R. Let ϕ_x and ϕ_z be the permeabilities of the porous facing in the x and z – directions, respectively. The region between the journal and porous facing is known as film region (having film thickness h) and is filled with FF lubricant. The origin O, the x – axis and the z – axis of the system is shown in

figure. Assume that the bearing is infinite along its axis lying along the $y-$ axis. Figure 5.2 shows the configuration of figure 5.1 opened up at *O*, where the circumference of the journal lies over $0 \le \theta \le 2\pi$ on the θ – axis and the film is symmetrical about the line $\theta = \pi$.

The basic flow equations other than equation (5.10) are given as follows.

Equation of continuity for the film region

$$\frac{\partial u}{\partial x} + \frac{\partial w}{\partial z} = 0 \tag{5.11}$$

Equation of Continuity for the porous region

$$\frac{\partial \bar{u}}{\partial x} + \frac{\partial \bar{w}}{\partial z} = 0 \tag{5.12}$$

Darcy's law for the porous region

$$\bar{u} = -\frac{\phi_x}{\eta}\left[\frac{\partial}{\partial x}\left(P - nk_{\mathrm{B}}T\ln\frac{\sinh\xi}{\xi}\right) - \frac{1}{4}\frac{\partial}{\partial z}\left(\mu_0 M_0 \bar{\tau} H\frac{\partial u}{\partial z}\right)\right], (x-\text{direction}) \tag{5.13}$$

$$\bar{w} = -\frac{\phi_z}{\eta}\left[\frac{\partial}{\partial z}\left(P - nk_{\mathrm{B}}T\ln\frac{\sinh\xi}{\xi}\right) + \frac{1}{4}\frac{\partial}{\partial x}\left(\mu_0 M_0 \bar{\tau} H\frac{\partial u}{\partial z}\right)\right], (z-\text{direction}) \tag{5.14}$$

where *u*, *w* are the velocity components in the film region, and $\bar{u}, \bar{w}$ are the velocity components in the porous region in the *x* and *z* – directions, respectively. Whereas *P* being the fluid pressure in the porous region.

Solving equation (5.10) under the boundary conditions

$$u = 0 \text{ when } z = 0$$

and

$$u = -\frac{1}{s}\frac{\partial u}{\partial z} \text{ when } z = h\,;\; s = \frac{5}{\sqrt{\phi_x \eta_x}} \text{ (slip boundary condition)}$$

implies

$$u = \left[\frac{(1+sh)z^2 - h(2+sh)z}{2\eta(1+\tau)(1+sh)} \right] \frac{d}{dx}\left(p - nk_B T \ln \frac{\sinh \xi}{\xi} \right), \tag{5.15}$$

where s is slip constant and η_x being the porosity in the x – direction.

Substituting equations (5.13) and (5.14) in equation (5.12), and integrating it with respect to z from h to $h + H^*$, yields

$$\phi_z \frac{\partial}{\partial z}\left(P - nk_B T \ln \frac{\sinh \xi}{\xi} \right)\Bigg|_{z=h}$$

$$= \phi_x H^* \frac{d^2}{dx^2}\left(P - nk_B T \ln \frac{\sinh \xi}{\xi} \right) + \frac{1}{4}(\phi_z - \phi_x) \frac{\partial}{\partial x}\left(\mu_0 M_0 \bar{\tau} H \frac{\partial u}{\partial z} \right)\Bigg|_h^{h+H^*} \tag{5.16}$$

using the fact that the surface $z = h + H^*$ is impermeable.

Substituting value of $\left(\frac{\partial u}{\partial z} \right)_h^{h+H^*}$ from equation (5.15), equation (5.16) becomes

$$\phi_z \frac{\partial}{\partial z}\left(P - nk_B T \ln \frac{\sinh \xi}{\xi} \right)\Bigg|_{z=h}$$

$$= \phi_x H^* \frac{d^2}{dx^2}\left(p - nk_B T \ln \frac{\sinh \xi}{\xi} \right) + \frac{1}{4\eta}(\phi_z - \phi_x) H^* \frac{d}{dx}\left[\frac{\mu_0 M_0 \bar{\tau} H}{1+\tau} \frac{d}{dx}\left(p - nk_B T \ln \frac{\sinh \xi}{\xi} \right) \right] \tag{5.17}$$

using Morgan-Cameron approximation [12,13].

Owing to the continuity of the fluid velocity components across the surface $z=h$,

$$w_{z=h} = \dot{h} + \bar{w}_{z=h},$$

implies

$$w_{z=h} = \dot{h} - \frac{\phi_z}{\eta}\left[\frac{\partial}{\partial z}\left(P - nk_B T \ln \frac{\sinh \xi}{\xi} \right) \right]_{z=h} - \frac{\phi_z}{8\eta} \frac{\partial}{\partial x}\left[\frac{4\tau s h^2}{(1+\tau)(1+sh)} \frac{d}{dx}\left(p - nk_B T \ln \frac{\sinh \xi}{\xi} \right) \right]$$

(5.18)

using equations (5.14) and (5.15). Here, $\dot{h}$ is squeeze velocity.

Integrating continuity equation (5.11) over the film thickness (0, *h*) and using equations (5.15), (5.17), (5.18), the Reynolds-Darcy equation for the present study can be obtained as

$$\frac{d}{dx}\left\{\left[12\phi_x H^* + \frac{h^3(sh+4)+6\phi_z\tau sh^2}{(1+\tau)(1+sh)} + \frac{12(\phi_z-\phi_x)H^*\tau}{1+\tau}\right]\frac{d}{dx}\left(p - nk_{\mathrm{B}}T\ln\frac{\sinh\xi}{\xi}\right)\right\} = 12\eta\dot{h} \tag{5.19}$$

using the fact that the surface z =0 is impermeable.

Using

$$x = R\theta,\ h = c(1+\varepsilon\cos\theta),\ \dot{\varepsilon} = \frac{d\varepsilon}{dt},\ \varepsilon = \frac{e}{c},$$

equation (5.19) can be expressed as

$$\frac{d}{d\theta}\left\{\left[12\phi_x H^* + \frac{h^3(sh+4)+6\phi_z\tau sh^2}{(1+\tau)(1+sh)} + \frac{12(\phi_z-\phi_x)H^*\tau}{1+\tau}\right]\frac{d}{d\theta}\left(p - nk_{\mathrm{B}}T\ln\frac{\sinh\xi}{\xi}\right)\right\} = 12\eta R^2 c\dot{\varepsilon}\cos\theta, \tag{5.20}$$

where c is radial clearance, e is eccentricity and $\varepsilon\,(0 \le \varepsilon \le 1)$is the eccentricity ratio .

Introducing the dimensionless quantities

$$\bar{s} = sc,\ \bar{h} = \frac{h}{c},\ \bar{p} = \frac{c^2 p}{\eta R^2\dot{\varepsilon}},\ \psi_x = \frac{H^*\phi_x}{c^3},\ \psi_z = \frac{H^*\phi_z}{c^3},\ \gamma = \frac{6\phi_z}{c^2},\ \mu^* = \frac{nc^2 k_{\mathrm{B}}T}{\eta R^2\dot{\varepsilon}}, \tag{5.21}$$

equation (5.20) reduces to

$$\frac{d}{d\theta}\left[G\frac{d}{d\theta}\left(\bar{p} - \mu^*\ln\frac{\sinh\xi}{\xi}\right)\right] = 12\cos\theta, \tag{5.22}$$

where

$$G = \frac{12(\psi_x + \psi_z \tau)}{1+\tau} + \frac{\bar{h}^3(\bar{s}\bar{h}+4) + \gamma\tau\bar{s}\bar{h}^2}{(1+\tau)(1+\bar{s}\bar{h})} \tag{5.23}$$

and

$$H^2 = kx(2\pi R - x) = kR^2\theta(2\pi - \theta) \Rightarrow H = \sqrt{k}R\sqrt{\theta(2\pi-\theta)}, \tag{5.24}$$

$$\xi = \frac{\mu_0 mH}{k_B T} = \frac{\mu_0 m}{k_B T}\sqrt{k}R\sqrt{\theta(2\pi-\theta)} = \lambda\sqrt{\theta(2\pi-\theta)};\ \lambda = \frac{\mu_0 m\sqrt{k}R}{k_B T}, \tag{5.25}$$

where k is a quantity chosen to suit the dimensions of both sides of equation (5.24).

It should be noted that the lubricant behaves as FF when there is an effect of magnetic field. So, in order to define FF effect $0 < \theta < 2\pi$.

5.3 Solution

Solving equation (5.22) under the boundary conditions

$$\frac{d\bar{p}}{d\theta} = 0 \text{ when } \theta = \pi \text{ and } \bar{p} = 0 \text{ when } \theta = 0 \tag{5.26}$$

yields

$$\bar{p} = \mu^* \ln\frac{\sinh\xi}{\xi} + 12\int_0^\theta \frac{\sin\theta}{G}\,d\theta. \tag{5.27}$$

If W_x and W_z are components of the load-carrying capacity W of the bearing, then

$$W = \sqrt{W_x^2 + W_z^2}, \tag{5.28}$$

where

$$W_x = LR\int_0^{2\pi} p\sin\theta d\theta = 0,\ W_z = LR\int_0^{2\pi} p\cos\theta d\theta,$$

where L is length of the bearing.

Using (5.21) and (5.26), dimensionless load-carrying capacity can be obtained as

$$\overline{W} = \frac{Wc^2}{LR^3\eta\dot{\varepsilon}} = \left| -\mu^* I^* - 12\int_0^{2\pi} \frac{\sin^2\theta}{G} d\theta \right|,$$

therefore,

$$\overline{W} = \mu^* I^* + 12\int_0^{2\pi} \frac{\sin^2\theta}{G} d\theta, \tag{5.29}$$

where

$$I^* = \lambda \int_0^{2\pi} (\pi - \theta) \frac{\sin\theta\left(\coth\xi - \frac{1}{\xi}\right)}{\sqrt{\theta(2\pi - \theta)}} d\theta. \tag{5.30}$$

5.4 Results and discussion

The results for the dimensionless load-carrying capacity $\overline{W}$ (given by equation (5.29)) are computed using Simpson's one-third rule with the step size of π/5. The representative values of the different parameters taken in computations are as follows [9, 10].

R = 0.002 m, k_B = 1.38 × 10^{-23} J (^{o}K)$^{-1}$, φ = 0.0075, V = 1.02 × 10^{-25} m^3

c = 2.5 × 10^{-5} m, $\dot{\varepsilon} = 0.1\,\mathrm{s}^{-1}$, $\eta_0 = 0.012$ N s m^{-2}, H^* = 0.00001 m, $\eta_x = 0.25$,

T = 297 ^{o}K, $\mu_0 m = 1.75\times10^{-25}$ J A^{-1} m, $\phi_z = 10^{-11}\mathrm{m}^2$,

$\phi_x = 10^{-12}\mathrm{m}^2$, $k = 10^{11}/3.95102(\mathrm{A}^2\mathrm{m}^{-4})$,

with the relations

$$\lambda = 0.3182(\xi)_{\max},\ \sqrt{k} = 0.3726\times10^7(\xi)_{\max}.$$

Also, for smaller values of ξ,

$$\coth\xi - \frac{1}{\xi} \to 0\,,\ \ \frac{\xi - \tanh\xi}{\xi + \tanh\xi} \to 0.$$

Moreover,

$$\lim_{\theta \to 0 \text{ or } 2\pi} \frac{(\pi-\theta)\sin\theta\left(\coth\xi - \frac{1}{\xi}\right)}{\sqrt{\theta(2\pi-\theta)}} \to 0.$$

The calculation of the order of magnetic field strength is shown below.

From equation (5.24),

$$H_{\max}^2 = 3.95102 \times 10^{-5} k$$

$$\text{For } H \approx O(10^3),\ k = 10^{11} / 3.95102,\ \lambda = 0.0136.$$

In the present analysis, FF is controlled by radially VMF (given by equation (5.24)), whose strength (intensity) H^2 is maximum at $\theta = \pi$. The order of magnetic field strength $O(H)$ for different values of *k* is shown in figure 5.3. It is observed that $O(H)$ increases with the increase of *k* whenever *R* is fixed.

The computed values of dimensionless load-carrying capacity $\overline{W}$ for different parameters are displayed graphically in figures 5.4-5.7.

The variation in $\overline{W}$ for different values of eccentricity ratio ε is shown in figure 5.4 for $\bar{H}^* = 0.4$. Three cases due to different permeabilities are discussed: $\psi_x < \psi_z$ (anisotropic case: ψ_x = 6.40E–04, ψ_z = 6.40E–03), $\psi_x = \psi_z$ (isotropic case: ψ_x = 6.40E–03, ψ_z = 6.40E–03), $\psi_x > \psi_z$ (anisotropic case: ψ_x = 6.40E–02, ψ_z = 6.40E–03), where ψ_x and ψ_z are dimensionless permeability parameters in the *x* and *z* – directions, respectively. From the figure 5.4, it is observed that for the anisotropic case $\psi_x < \psi_z$ and $\psi_x = \psi_z$, the dimensionless load carrying capacity $\overline{W}$ increases significantly with the increase of ε with almost the same behaviour. This behaviour is due to the formation of capillaries. For instance, in the anisotropic case of

$\psi_x < \psi_z$, permeability in the $z-$ direction is higher than the $x-$ direction. Therefore, formation of capillaries in the $z-$ direction, that is perpendicular to film region are higher than in the $x-$ direction, that is parallel to outward radial direction. Hence, fluid easily flows to the film region, which results in to higher load carrying capacity $\overline{W}$. The load carrying capacity $\overline{W}$ increases moderately with the increase of ε for the anisotropic case $\psi_x > \psi_z$. The increase is almost linear. This is due to the fact that capillaries formation in the $x-$direction is higher than in the $z-$ direction. Therefore, less fluid flows in to the film region. Thus, in this case porosity has no significant impact on the load carrying capacity.

Figure 5.5 shows the variation of $\overline{W}$ against the variation of dimensionless porous thickness parameter $\bar{H}^*(=H^*/c)$ From the figure 5.5, it should be noted that increase of $\overline{W}$ for the anisotropic case $\psi_x < \psi_z$ becomes more significant when the thickness of the porous matrix is thin. Here ε = 0.7, ψ_x = 6.40E−04 and ψ_z = 6.40E−03 are fixed for this case. It is observed that as $\bar{H}^*$ increases, the load carrying capacity $\overline{W}$ decreases rapidly.

From the figure 5.6, it should be noted that dimensionless permeability parameter ψ_x has significant impact on $\overline{W}$. Figure 5.6 shows the variation in $\overline{W}$ against variation of dimensionless permeability parameter ψ_x when $\psi_x < \psi_z$ for ψ_z = 6.40E−03, ε = 0.7 and $\bar{H}^* = 0.4$. It is observed that as we decrease the value of ψ_x the dimensionless load carrying capacity $\overline{W}$ increases. This implies that load carrying capacity $\overline{W}$ can be increased by further decreasing the value of ψ_x < 6.40E−04.

Figure 5.7 shows the variation in dimensionless load carrying capacity against the variation of dimensionless permeability parameter ψ_x when $\psi_x > \psi_z$ for ψ_z = 6.40E−03, ε = 0.7 and $\bar{H}^* = 0.4$. Here, it should be noted that as ψ_x moves from 6.40E−02 to 6.40E+02, there is

sudden decrease in dimensionless load carrying capacity $\overline{W}$. This is due to the fact as discussed earlier that formation of capillaries in outward radial direction is higher than capillaries which are almost perpendicular to the film region. Therefore, capillaries in outward radial direction retains more fluid and hence fluid flows in the film region is less.

5.5 Conclusions

In this chapter the case of porous journal bearing is studied with the effects of squeeze velocity, anisotropic permeability and slip velocity. The modified Reynolds-Darcy equation for porous journal bearing is derived considering continuity equation in the film as well as porous region and by assuming the validity of the Darcy's law in the porous region. The expression for dimensionless load-carrying capacity is obtained and studied for different parameters. The results and discussion shows the following observations.

(1) The order of magnetic field strength O (H) increases with the increase of k.

The dimensionless load-carrying capacity $\overline{W}$

(2) increases, in general, with the increase of eccentricity ratio ε.

(3) performed best for the anisotropic case $\psi_x < \psi_z$ and then for isotropic case $\psi_x = \psi_z$, with the same behaviour. The increase rate of $\overline{W}$ is more significant for both the cases when $\varepsilon > 0.1$.

(4) increases linearly and moderately with the increase of ε for the anisotropic case $\psi_x > \psi_z$.

(5) increases with the decrease of dimensionless porous thickness parameter $\bar{H}^*$ for $\psi_x < \psi_z$.

(6) decreases rapidly with the increase of $\bar{H}^*$ for $\psi_x < \psi_z$.

(7) increases with the decrease of ψ_x for $\psi_x < \psi_z$.

(8) decreases suddenly as ψ_x moves from 6.40E−02 to 6.40E+02 for $\psi_x > \psi_z$.

Thus, the dimensionless load-carrying capacity $\overline{W}$ increases with the increase of eccentricity ratio ε and the effect of magnetic field, and performed best for the anisotropic case $\psi_x < \psi_z$ with the decrease of ψ_x for thin layer of porous matrix.

References

1. Kuzhir, P. 2008 Free boundary of lubricant film in ferrofluid journal bearings. Tribology International, 41: 256–268.
2. Patel, NS, Vakharia DP, Deheri GM. 2012 A study on the performance of a magnetic-fluid-based hydrodynamic short journal bearing. ISRN Mechanical Engineering, Article ID 603460, 7 pages.
3. Lin JR, Li PJ, Hung TC. 2013 Lubrication performances of short journal bearings operating with non-Newtonian ferrofluids. Z. Naturforsch, 68a: 249–254.
4. Hsu TC, Chen JH, Chiang HL, Chou TL. 2014 Combined effects of magnetic field and surface roughness on long journal bearing lubricated with ferrofluid. Journal of Marine Science and Technology, 22(2): 154–162.
5. Rao TVVLN, Rani AMA, Nagarajan T, Hashim F. 2016 Analysis of porous layered journal bearing lubricated with ferrofluid. Applied Mechanics and Materials, 819: 474–478.
6. Hu R, Xu C. 2017 Influence of magnetic fluids' cohesion force and squeeze dynamic effect on the lubrication performance of journal bearing. Advances in Mechanical Engineering, 9(9): 1–13.
7. Laghrabli S, Khlifi EM, Nabhani, M, Bou-Saïd, B. 2017 Ferrofluid lubrication of finite journal bearings using Jenkins model. Lubrication Science, 29: 441–454.
8. Shliomis MI. 1972 Effective viscosity of magnetic suspensions. Soviet Physics JETP, 34(6): 1291–1294.
9. Shah RC, Bhat MV. 2005 Ferrofluid squeeze film between curved annular plates including rotation of magnetic particles. Journal of Engineering Mathematics, 51(4): 317–324.
10. Shah RC, Shah RB. 2017 Ferrofluid lubrication of circular squeeze film bearings controlled by variable magnetic field with rotations of the discs, porosity and slip velocity. Royal Society Open Science, 4: 170254.
11. Shliomis MI. 1974 Magnetic fluids. Soviet Physics Usp., 17(2): 153–169.
12. Shah RC, Bhat MV. 2004 Anisotropic permeable porous facing and slip velocity on squeeze film in an axially undefined journal bearing with ferrofluid lubricant. Journal of Magnetism and Magnetic Materials, 279: 224–230.

13. Sparrow EM, Beavers GS, Hwang IT. 1972 Effect of velocity slip on porous-walled squeeze films. Journal of Lubrication Technology, 94(3): 260–265.

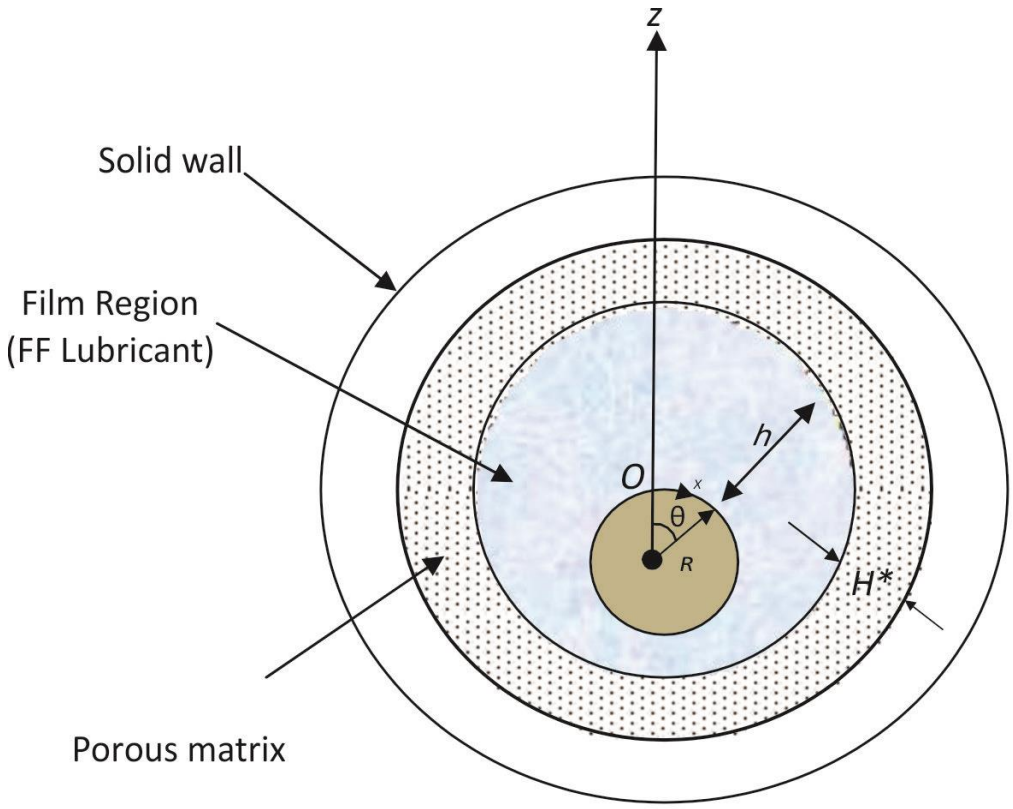

Figure 5.1. Porous journal bearing.

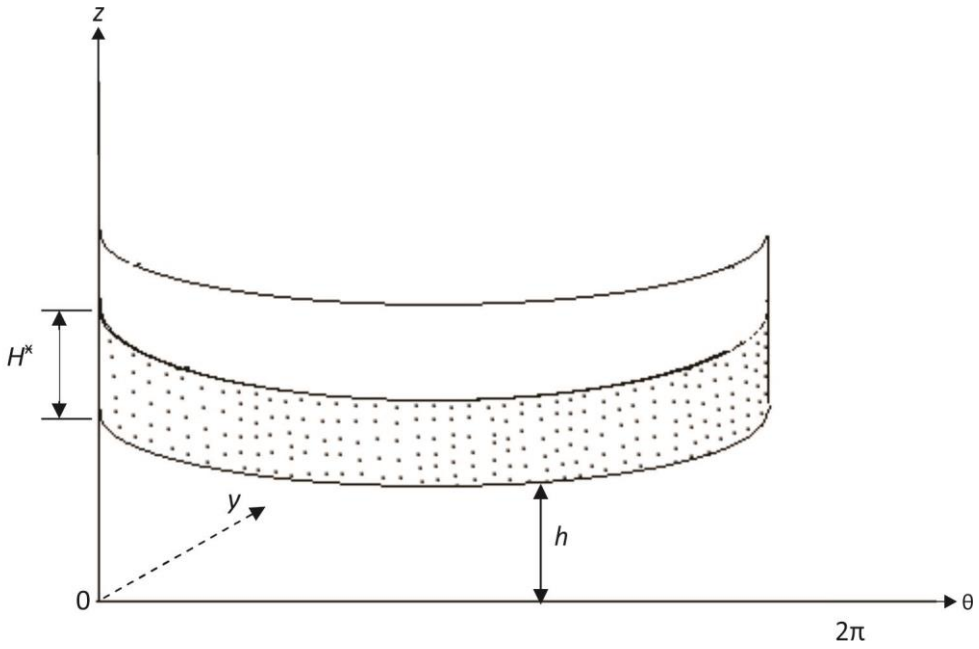

Figure 5.2 Configuration of figure 5.1 opened up at *O*

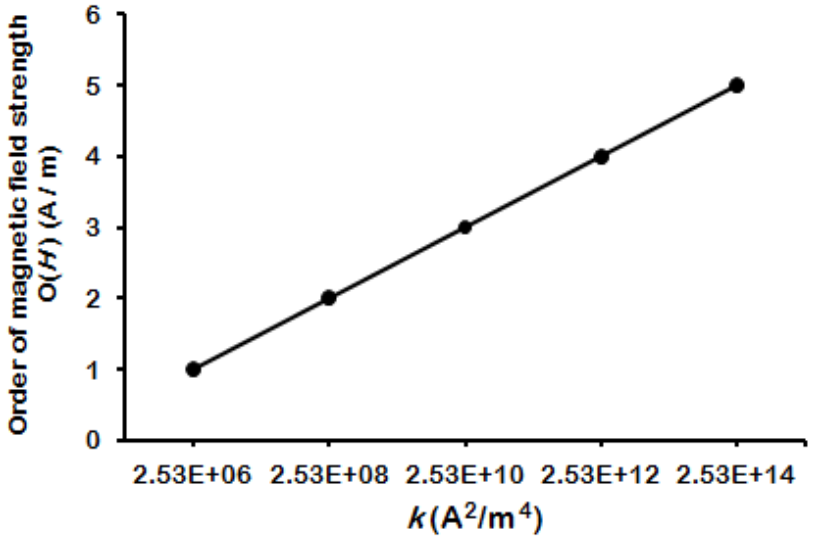

Figure 5.3 Order of magnetic field strength for different values of *k*

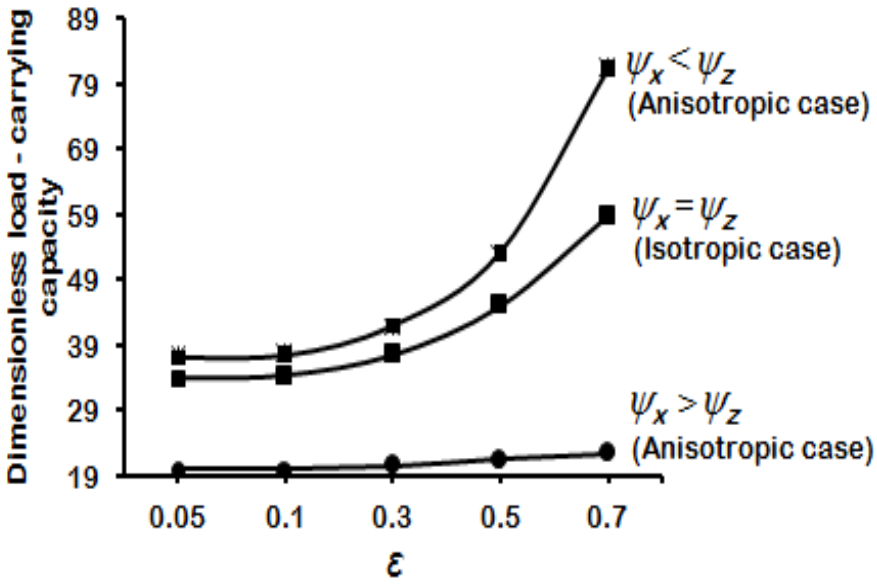

Figure 5.4 Variation in dimensionless load-carrying capacity $\overline{W}$ for different values of eccentricity ratio ε for $\psi_x<\psi_z$ (ψ_x = 6.40E–04, ψ_z = 6.40E–03), $\psi_x=\psi_z$ (ψ_x = 6.40E–03, ψ_z = 6.40E–03), $\psi_x>\psi_z$ (ψ_x = 6.40E–02, ψ_z = 6.40E–03) and $\bar{H}^* = 0.4$.

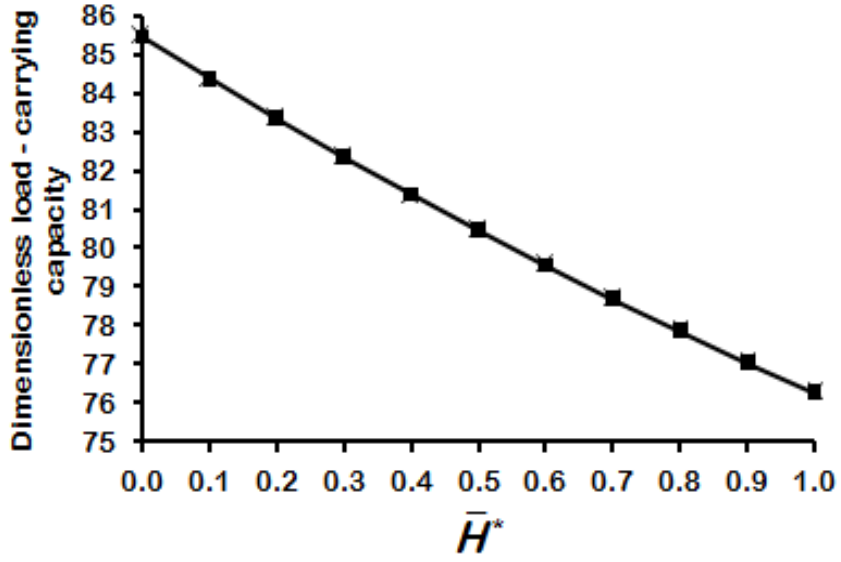

Figure 5.5 Variation in dimensionless load-carrying capacity $\overline{W}$ for different values of dimensionless porous thickness parameter $\bar{H}^*(=H^*/c)$ for ε = 0.7, ψ_x = 6.40E–04, ψ_z = 6.40E–03

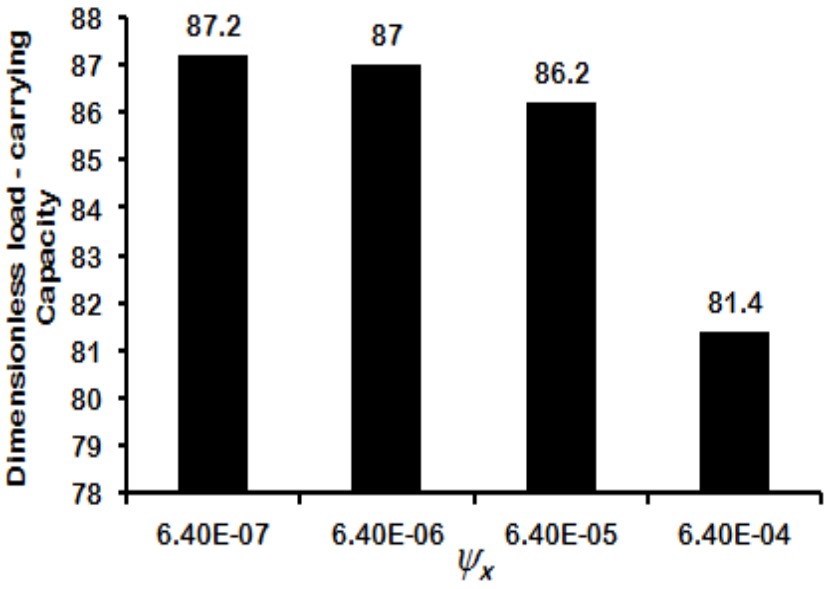

Figure 5.6 Variation in dimensionless load-carrying capacity $\overline{W}$ for different values of dimensionless permeability parameter ψ_x when $\psi_x < \psi_z$ (ψ_z = 6.40E–03) and for ε = 0.7, $\bar{H}^* = 0.4$.

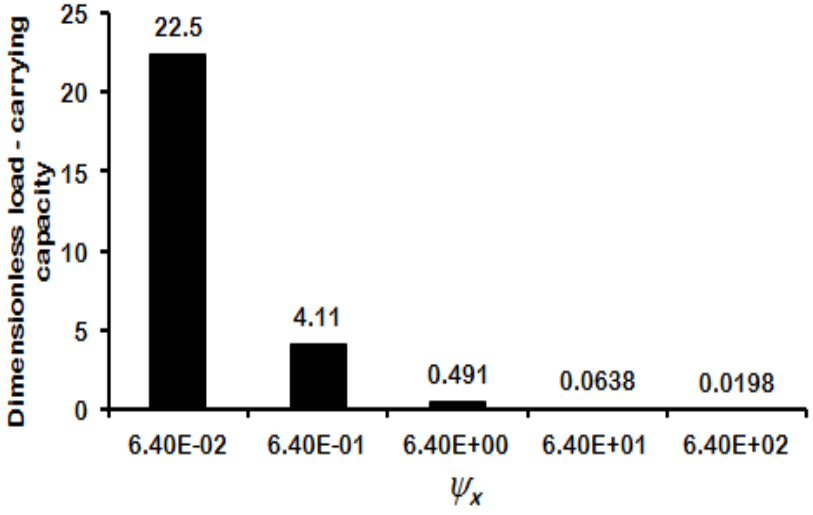

Figure 5.7 Variation in dimensionless load-carrying capacity $\overline{W}$ for different values of dimensionless permeability parameter ψ_x when $\psi_x > \psi_z$ (ψ_z = 6.40E–03) and for ε = 0.7, $\bar{H}^* = 0.4$.